A simplified model of precipitation enhancement over a heterogeneous surface

Guido Cioni[1,2,3] and Cathy Hohenegger[1,3]

[1]Max Planck Institute for Meteorology, Hamburg, Germany
[2]International Max-Planck Research School on Earth System Modelling
[3]Hans-Ertel-Zentrum for Weather Research

Correspondence to: Guido Cioni (guido.cioni@mpimet.mpg.de)

Abstract. Soil moisture heterogeneities influence the onset of convection and subsequent evolution of precipitating systems through the triggering of meso-scale circulations. However, local evaporation also plays a role in determining precipitation amounts. Here we aim at disentangling the effect of advection and evaporation on precipitation over the course of a diurnal cycle by formulating a simple conceptual model. The derivation of the model is inspired from the results of simulations performed with a high-resolution (250 m) Large-Eddy Simulation model over a surface with varying degrees of heterogeneity. A key element of the conceptual model is the representation of precipitation as weighted sum of advection and evaporation, each weighted by its own efficiency. The model is then used to isolate the main parameters that control the variations of precipitation over a spatially drier patch. It is found that these changes surprisingly do not depend on soil moisture itself but instead purely on parameters that describe the atmospheric initial state. The likelihood for enhanced precipitation over drier soils is discussed based on these parameters. Additional experiments are used to test the validity of the model.

1   Introduction

Will a wetter soil lead to more or less precipitation? This apparently simple question inspired many studies over the course of the last 50 years. Over a homogeneous surface precipitation is expected to increase with surface evaporation, and thus with soil moisture in a soil moisture-limited regime (Manabe, 1969; Budyko, 1974), regardless of the atmospheric state (Cioni and Hohenegger, 2017) as long as convection can be triggered on both dry or wet surfaces (Findell and Eltahir, 2003). However, the real world is far from being homogeneous. The presence of heterogeneity in surface soil moisture induces thermally-driven meso-scale circulations (Segal and Arritt, 1992) which transport moist air from spatially wetter patches to spatially drier patches, acting against the initial perturbation of soil moisture, and which can then affect the distribution of precipitation.
Many idealized studies have investigated the effect of such circulations on convection and ensuing precipitation. Avissar and Liu (1996) found that the land-surface wetness heterogeneity (i.e. spatial gradients of soil moisture) controls the transition from a randomly scattered state of convection to a more organized one where clouds form ahead of the front associated with the meso-scale circulation. The presence of such circulations also tend to enhance the precipitation amount. Further analyses have shown that this basic response can be modified by many environmental factors.
Yan and Anthes (1988) found that accumulated precipitation is maximized over spatially dry patches when the patch length is

comparable to the local Rossby radius of deformation (~ 100 km in mid-latitudes), a result that was later confirmed by Chen and Avissar (1994) and Lynn et al. (1998). Robinson et al. (2008) proposed an alternative explanation by which the effect of surface hot spots is maximized for wavelength of roughly 50 km, that is when the aspect ratio of the applied heating matches the ratio of vertical and horizontal wavenumbers demanded by the dispersion relation for buoyancy (gravity) waves.

5 Froidevaux et al. (2014) explored the interaction between horizontal soil moisture variations, wind and precipitation. They found that, only when winds are too weak to control the propagation of thunderstorms, more precipitation is observed over drier surfaces. Finally, the response of precipitation also depends upon the background atmospheric profile. Chen and Avissar (1994) found that the presence of a moist atmospheric profile over a spatially drier surface reduces the precipitation advantage as the surface heat fluxes, which drive the surface heating and thus the circulation, are reduced. Hence, from such studies,

10 an increase of precipitation over spatially drier patches is maximized when the gradient of surface wetness is high, the soil moisture heterogeneity length-scale is around 50-100 km and no background wind is present.

These same mechanisms can be observed in some areas of the world, the so-called hot spots of land-atmosphere interactions (Koster et al., 2004). Several observational studies (e.g. Taylor et al. (2012)) showed that in the Sahel region thunderstorms occur preferably over regions drier than their surroundings. In other areas of the world the synoptic forcing is usually so strong

15 that a robust relationship of causality between soil moisture and precipitation cannot be found (Tuttle and Salvucci, 2017). Instead of speaking of heterogeneous or homogeneous conditions, Guillod et al. (2015) have indicated that over most areas of the world, except the Sahel, a negative spatial coupling coexists together with a positive temporal coupling. That is, areas drier than their surrounding (spatial component) but wetter than the climatological value (temporal component) may receive more precipitation than other ones.

20 Although the aforementioned studies have qualitatively shown how precipitation is influenced by soil moisture, soil moisture gradients and by the atmospheric environment, here we aim at developing a simplified conceptual model to formally isolate the control of soil moisture on precipitation. In particular we aim at developing a mathematical expression for the derivative of precipitation with respect to soil moisture in the case of a heterogeneous surface to understand the response of precipitation to soil moisture changes. In this case, precipitation is not only affected by the advection of moisture due to the meso-scale

25 circulation but also by local evaporation (Wei et al., 2016). These two factors depend differently on soil moisture.

The meso-scale circulation triggered by the surface wetness heterogeneity strengthens with decreasing soil moisture of the dry patch, as this gives a larger spatial gradient of surface heat fluxes and thus of surface pressure. Instead local evaporation is limited with reduced local soil moisture. The superposition of local evaporation and remote moisture advection eventually contribute to the observed precipitation, with the atmosphere being the medium that weights these two different contributions.

30 Lintner et al. (2013) already derived an equation for the derivative of precipitation with respect to soil moisture based on a model of intermediate-level complexity of the tropical atmosphere (Quasi-equilibrium Tropical Circulation Model 1 (QTCM1), Neelin and Zeng (2000)). Inspired by their work, we develop a theoretical model which is based on similar assumptions but simplifies the formulation of moisture advection and evaporation. In particular the fact that we consider the specific case of advection by a thermally-induced meso-scale circulation, and not by the large-scale flow, will allow us to greatly simplify the

35 idealized framework.

Section 2 describes the model and experimental set-up that allows us to simulate the evolution of convective clouds and precipitation over a heterogeneous land-surface during a diurnal period. After a brief analysis of the features of the convective diurnal cycle in section 3.1 we estimate the various terms of the moisture balance and in particular the efficiencies of the conversion of evaporation and advection into precipitation in section 3.2. These results are used in section 4 to derive a simple conceptual model of how precipitation responds to soil moisture changes over a heterogeneous surface. We will show that, at least to a first order, the change of precipitation with soil moisture does not depend on the soil moisture content itself but only on the atmospheric state. The results are concluded in section 5.

2 Methods

The modeling framework used in this work is, in terms of physical parametrizations and dynamical core, identical to the one described in Cioni and Hohenegger (2017), to which the reader is referred for details. We use the ICOsahedral Non-hydrostatic - Large Eddy Model (ICON-LEM) as atmospheric model coupled to the land-surface model, TERRA-ML, to simulate the diurnal cycle of convection over idealized land surfaces from 6 Local Standard Time (LST) to 24 LST.

The horizontal periodic domain spans 1600×400 points with a resolution (in terms of the triangle edges, see Zängl et al. (2015)) of 250 m, which results in a size of approximately 400×100 km^2. In the vertical dimension 150 levels are distributed from the surface up to the model top located at 21 km: the spacing reaches 20 m in the lower levels and 400 m close to the model top. In contrast to Cioni and Hohenegger (2017), heterogeneous surface conditions are used as bottom boundary condition. The heterogeneity is prescribed by dividing the domain's x-direction into two patches having the same surface area of 200×100 km^2. Figure 1 displays a sketch of the domain setup, together with a visual representation of convective features that will be discussed later.

The domain is rectangular in order to limit computational expenses and is elongated in the x-axis given that the front associated with the simulated meso-scale circulation is expected to propagate with a direction parallel to the x-axis. The chosen patch size of 200 km is larger than the optimal value of the heterogeneity wavelength (~ 100 km) identified by Chen and Avissar (1994); Yan and Anthes (1988); Lynn et al. (1998). Therefore we do not expect to maximize, in terms of the strength of the meso-scale circulation, the response of the atmosphere to the surface heterogeneity. This could eventually reduce the dynamic contribution of advection on precipitation. The larger domain has nevertheless the advantage that the opposite fronts collide later in the day so that the daily precipitation amounts are less affected by what happens after the fronts have collided. The sensitivity of the diurnal evolution of precipitation to different y-axis size was tested, and found to not affect the results.

The surface heterogeneity is introduced by setting two different initial values of volumetric soil moisture ϕ [m^3 m^{-3}] for the two patches, ϕ_{wet} and ϕ_{dry}, respectively. The value is set to the entire soil column to ease the interpretation of the results. The other parameters that characterize the land surface, including e.g. soil temperature, are horizontally homogeneous over the entire domain. Initially the soil temperature is prescribed using a linear profile which includes a climatological layer with a temperature of 281 K at 14.58 m below the surface and a surface layer which has the same temperature as the overlying lowermost level of the atmosphere (see Cioni and Hohenegger (2017)).
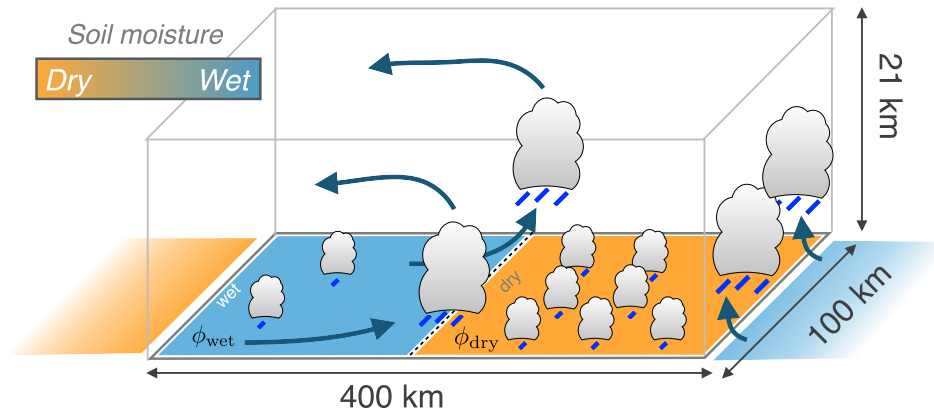
Figure 1. Sketch of the employed experimental framework. The initial condition for soil moisture and the expected initial development of convection are also sketched in order to ease the interpretation of the results.

The atmospheric initial state is spatially homogeneous except for random perturbations added to the vertical velocity and the virtual potential temperature in the lowermost three levels to break the perfectly symmetric initial state. The atmosphere is initialized using the dry-soil advantage profile of Findell and Eltahir (2003), albeit with winds set to zero to simplify the analysis (see Fig. 2). This sounding, indicated throughout the manuscript as DA, was observed on 23 July 1999 in Lincoln
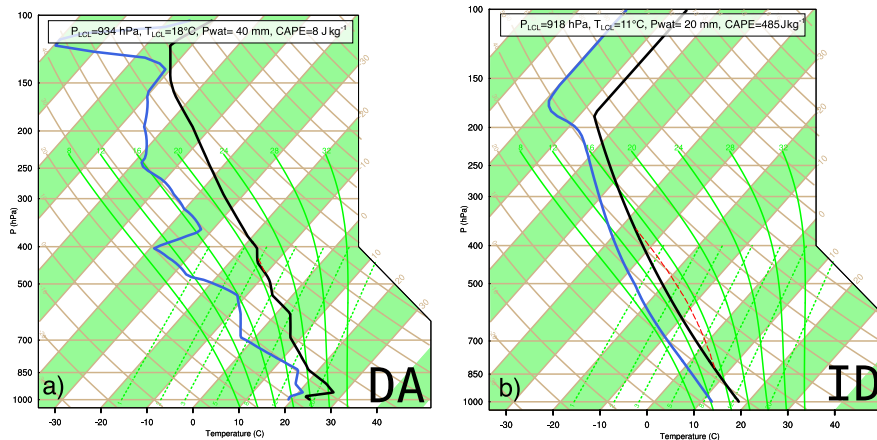
Figure 2. Skew-T diagrams of the two soundings used to initialize the atmosphere in the simulations. Panel (a) shows the dry soil advantage sounding of Findell and Eltahir (2003), DA, while panel (b) shows the idealized sounding of Schlemmer et al. (2012), ID. The upper inset in both panels show the value of pressure at the Lifted Condensation Level (LCL), temperature at the LCL, precipitable water and Convective Available Potential Energy (CAPE).

5 (Illinois, USA) and was chosen as a typical example by Findell and Eltahir (2003) for cases when a strong heating of a

homogeneous surface favors the triggering of convection.

To study the response of precipitation to variations in soil moisture, we perform a set of experiments by setting at the initial time ϕ_{wet} to the saturation value and varying ϕ_{dry}, with values ranging from the saturation to 20% of the saturation value. The latter value is below the wilting point for the chosen soil type (loam). More details about the soil type can be found in Cioni and Hohenegger (2017) and Doms et al. (2011). The upper part of Tab. 1 summarizes the simulations performed with this basic configuration.

In order to test the validity of the theory proposed in section 4 based on this set of basic experiments we perform further

Experiment	Sounding	ϕ_{dry}	ϕ_{wet}
Basic configuration			
DA_20_100	DA	20	100
DA_30_100		30	100
DA_40_100		40	100
DA_50_100		50	100
DA_60_100		60	100
DA_65_100		65	100
DA_70_100		70	100
DA_80_100		80	100
DA_100_100		100	100
Not-saturated wet patch			
DA_20_70	DA	20	70
DA_30_70		30	70
DA_40_70		40	70
DA_50_70		50	70
DA_60_70		60	70
DA_70_70		70	70
Idealized sounding			
ID_20_100	ID	20	100
ID_100_100	ID	100	100

Table 1. Overview of the performed simulations. The first column indicates the experiment name, whereas the second column indicates the sounding used for initialization: DA for dry soil advantage, after Findell and Eltahir (2003), and ID for idealized, after Schlemmer et al. (2012). Third and fourth columns indicate the value of soil moisture over the dry and wet patches, respectively, in percentage of the saturation value. Naming convention for the experiments follows SOUNDING_ϕ_{dry}_ϕ_{wet}. The vertical lines that characterize the ID cases are used to omit the repetition of the same experiments description, i.e. ID_30_100, ID_40_100, etc. .

sensitivity experiments. First, we decrease the initial value of ϕ_{wet} to 70 % of the saturation value. Second, we change the

initial atmospheric profile. We tested the wet soil advantage sounding of Findell and Eltahir (2003) where, in contrast to the dry soil advantage sounding, convection triggering requires a strong moistening of the boundary layer. We also tested the sounding of Schlemmer et al. (2012), indicated as `ID`, which represents an idealization of the typical atmospheric state prone to convection in Europe (see Fig. 2 b). This sounding thus greatly differs from the conditions as observed in Lincoln. It has

5   a lower surface temperature, a lower integrated water vapour content but a larger initial instability. As the use of the wet soil advantage sounding of Findell and Eltahir (2003) yields very similar results as in `DA`, which is not the case when using `ID`, we only report here on the `ID` simulations.

3   Results

3.1   General features of convection

10   Here, we describe the general features of the extreme case, `DA_20_100`, which reproduces the features expected from this kind of simulations. The differential heating of the two patches, caused by the heterogeneity in soil moisture, manifests itself in a gradient of both sensible and latent heat fluxes. At 12 LST the difference in sensible heat flux between the two patches reaches almost 280 W m^{-2}. This results in a difference in near-surface virtual potential temperature of about 4 K at the same time (see the colored contours in Fig. 3). As a consequence, a pressure gradient of about 1 hPa develops close to the surface,

15   which supports a thermally-driven circulation (Segal and Arritt, 1992). The circulation is constituted by a front of moist air moving inland over the dry patch at lower levels (from the surface up to 1 km) and a return flow between 1 and 3 km, as shown by the wind vectors in Fig. 3. As a result of the circulation, and as found in past studies, convection preferentially develops over the dry patch and in particular at the edge of the front associated with the meso-scale circulation.

In order to track the front associated with the meso-scale circulation we use an algorithm designed to follow one of the front

20   moving over the dry patch. The algorithm is based on the y-averaged zonal wind speed at 150 m of height. It is triggered when the wind speed in the middle of the domain reaches 1 m s^{-1} and automatically stops when the opposite fronts collide in the center of the dry patch. At every output time step (15 minutes) a search of the maximum value of zonal wind speed is performed in a box which is suitably chosen in order to maintain the focus of the tracking algorithm on the front. More specifically, at the first two time instants the maximum is searched over the entire dry patch while from the third time step

25   onward the maximum search is performed in a box centered on a first guess obtained from a simple linear extrapolation of the previous time instants. The size of the box is the only parameter that needs to be tuned when tracking the front in different simulations. Otherwise, the algorithm is robust. As an example, in the `DA_20_100` case shown in Fig. 4, the box comprises 5 grid points, thus approximately 1.25 km.

Figure 4 (a) shows the Hovmöller diagram of the zonal wind and the tracked position of the front every 15 minutes with

30   shaded circles for the case `DA_20_100`. In Fig. 4 (b) the position and speed of the front obtained with the aforementioned algorithm are displayed. The front starts to slowly propagate in the late morning with a velocity smaller than 2 m s^{-1} but is later accelerated by cold pools, in agreement with Rieck et al. (2015). The cold pools are formed after the first strong precipitation event between 12 and 13 LST. The speed of the front reaches values of up to 7 m s^{-1} before the front collides with the opposing
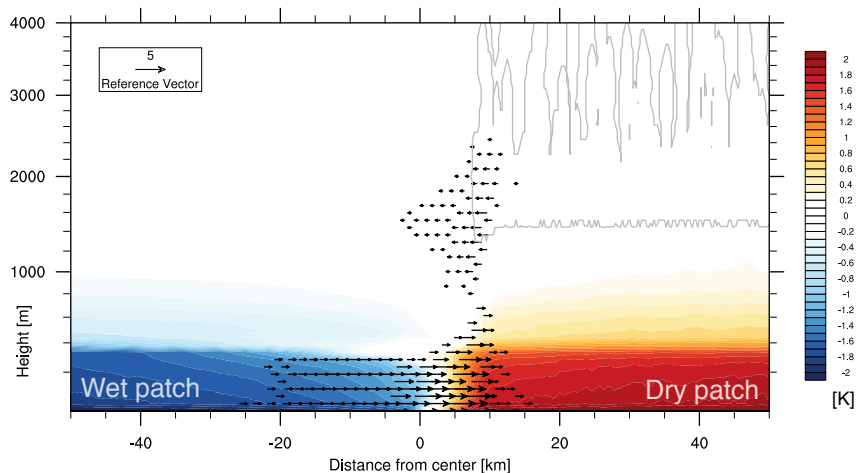
Figure 3. x-z diagram at 1200 LST of y-averaged quantities for the `DA_20_100` case. Zonal temperature anomaly (color contours), zonal wind (vectors, values between -0.5 and 1 m s^{-1} are masked) and cloud water mixing ratio (grey contour, only 10^{-5} g kg^{-1} isoline). On the x-axis numbers indicate the distance from the center of the domain in km.

front coming from the outer boundary due to the periodic domain. When the soil moisture of the dry patch exceeds 70% of the saturation value no circulation forms because the gradient in surface temperature is too weak to cause a pressure difference between the patches. In this case the convection transitions to a randomly scattered state (Avissar and Liu, 1996) and we define the speed of the front to be 0 m s^{-1}.

3.2 Local and remote sources of precipitation

The diurnal cycle of precipitation can be inspected and compared to the one of evaporation and advection, using the methodology introduced in appendix A. This is needed to later formally express precipitation as function of soil moisture (see section 4). Figure 5 shows the various components of the moisture balance computed every 5 minutes from the model output and averaged over the dry patch as well as over the entire domain. It can be verified that the advection term averaged over the entire domain is zero, as expected. Instead, when considering the residual averaged over the dry patch, A_{dry}, it is always positive, indicating a net transport of moisture from the wet to the dry patch.

The advection of moisture over the dry patch increases in the late morning as a result of the propagation of the front (see Fig. 4) and reaches a maximum at around 13 LST. This behavior is similar to the one observed by Yan and Anthes (1988, their Fig. 9). The first deep convection event in `DA_20_100` between 12 and 13 LST produces a strong cold pool which causes a strong surface divergence, explaining the minimum at about 14 LST in Fig. 5. Given that the maximum of precipitation associated with this event is located in the vicinity of the boundary between the wet and the dry patch, this induces a net negative effect on A_{dry}.

In order to study the variation of the moisture budget terms as function of ϕ_{dry} we conduct the same moisture balance anal-
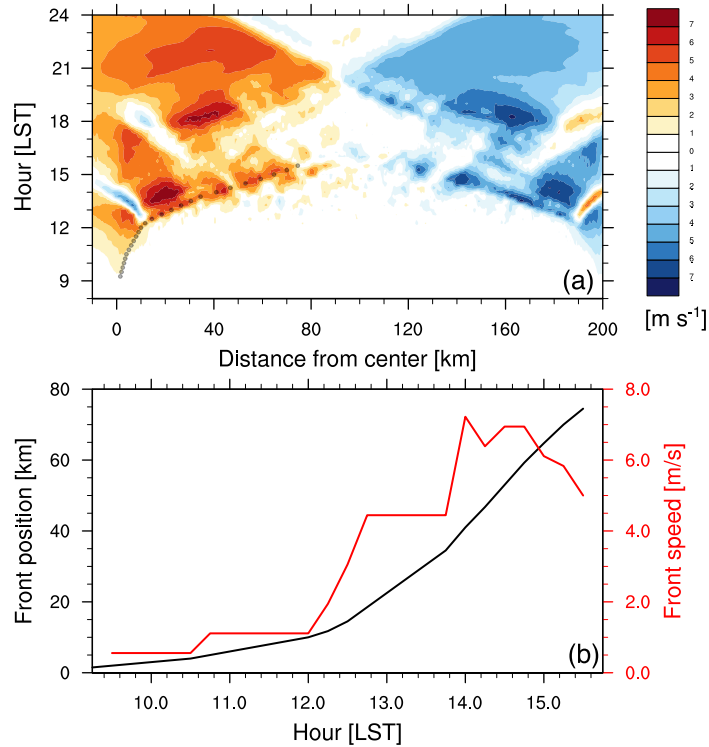
Figure 4. Tracking of the front associated with the meso-scale circulation for the case `DA_20_100`. (a) Hovmöller diagram (distance from domain center vs. time) of the y-averaged zonal wind at a height of 150 m above the surface. Dots indicate the position of the front tracked every 15 minutes (see text for details). (b) Front inland propagation (black line) with respect to the center of the domain [km] and front speed (red line) derived using finite differences [m s^{-1}].

ysis for every simulation and integrate the values over the entire diurnal cycle (18 hours). Results are reported in Tab. 2. As expected the advection term decreases with increasing local soil moisture whereas local evaporation increases. Overall the accumulated precipitation averaged over the dry patch decreases when the soil moisture increases, as shown also in Fig. 6. The sharp decrease of precipitation with increasing value of soil moisture seems to suggest that advection and evaporation are

5 characterized by different weights when producing precipitation. In fact, if the contribution of these processes would be the same, we would expect to observe a flattening of the precipitation values (blue asterisks in Fig. 6) instead than a decrease. In other words, advection appears to be more efficient than evaporation in producing precipitation, as the increase of E_{dry} with soil moisture is followed by a sharp decrease of P_{dry}.

These qualitative observations can be formalized by defining precipitation efficiencies. This approach was first proposed by

10 Budyko (1974) and later adopted by many studies including the one of Schär et al. (1999). The overall assumption underlying the pioneering work of Budyko (1974) is that moisture coming from inside (local evaporation) or outside (remote advection)
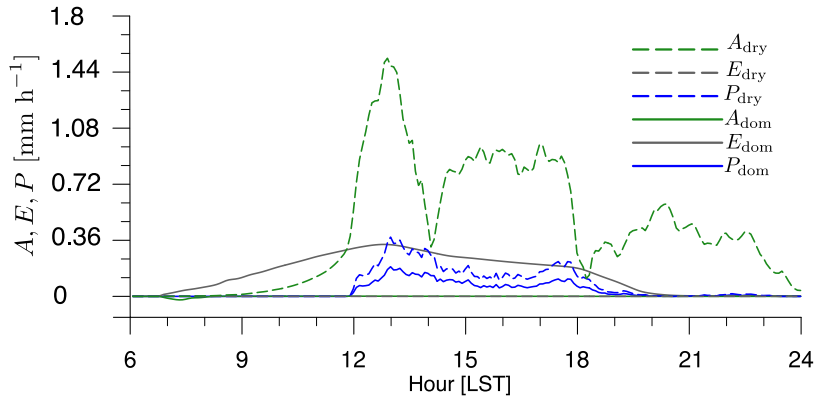
Figure 5. Different terms of the moisture balance (Eq. A3) computed for the entire domain (subscript $_{\text{dom}}$, solid lines) and for the dry patch (subscript dry, dashed lines) in the `DA_20_100` case. A indicates advection, E evaporation and P precipitation. Units are mm h^{-1}. Note that all variables in this figure are instantaneous.

Case	ϕ_{dry}	A_{dry}	E_{dry}	P_{dry}	η
DA_20_100	0.0908	7.796	0.0008	1.255	0.161
DA_30_100	0.1362	7.467	0.0113	1.077	0.144
DA_40_100	0.1816	7.223	0.1140	1.005	0.137
DA_50_100	0.2270	6.673	0.6373	0.912	0.125
DA_60_100	0.2724	4.665	2.0271	0.888	0.133
DA_65_100	0.2951	3.222	3.0393	0.805	0.129
DA_70_100	0.3178	1.734	4.0920	0.708	0.122
DA_80_100	0.3632	-0.412	5.2770	0.533	0.094
DA_100_100	0.4540	0.031	5.0800	0.560	0.110

Table 2. Values of soil moisture [m^3 m^{-3}], advection [mm], evaporation [mm] and precipitation [mm] over the dry patch accumulated over the diurnal cycle. The rightmost column shows the precipitation efficiency (dimensionless) computed as $\frac{P_{\text{dry}}}{A_{\text{dry}}+E_{\text{dry}}}$.

of some closed domain is well mixed. Under this assumption one can express the precipitation over a certain area as:

$$P_{\text{area}} = \eta(A_{\text{area}} + E_{\text{area}}) \tag{1}$$

where η is the precipitation efficiency. All the terms are considered as areal averages and integrated over a certain time period. The rightmost column of Tab. 2 shows the efficiency η computed according to Eq. 1. It can be seen that, in this case, convection is not so efficient in converting local and remote sources of moisture into precipitation as the values range from 16% to 9%. More importantly, the efficiency values vary by up to 7% depending on the initial ϕ_{dry}. In fact, in the case `DA_20_100`, evaporation over the dry patch is negligible, i.e. $E_{\text{dry}} \simeq 0$, so that Eq. 1 applied to the dry patch reads $P_{\text{dry}} \simeq \eta A_{\text{dry}}$. Thus, the efficiency obtained in this case is representative of the advection process and can be interpreted as an *advection efficiency* η_A.
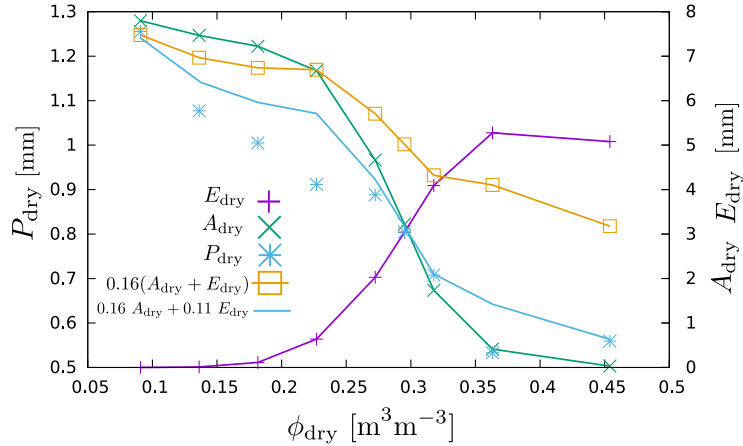
Figure 6. Values of advection (green line and crosses), evaporation (purple line and plus symbols) and precipitation (blue asterisks) from Tab. 2 as function of soil moisture. The orange line represents an estimate of precipitation obtained as a sum of advection and evaporation weighted by the same efficiency, i.e. $0.16(A_{\mathrm{dry}} + E_{\mathrm{dry}})$ while the blue line represents a similar estimate obtained by using two different efficiencies, i.e. $0.16\,A_{\mathrm{dry}} + 0.11\,E_{\mathrm{dry}}$.

On the other hand, in `DA_100_100` the advection is negligible so that in this case we obtain an *evaporation efficiency* η_E. Taking all these findings together, we rewrite Eq. 1 as:

$$P_{\mathrm{area}} = \eta_A \cdot A_{\mathrm{area}} + \eta_E \cdot E_{\mathrm{area}} \tag{2}$$

where now $\eta_A \neq \eta_E$. The values estimated from Tab. 2 are $\eta_A = 0.16$ and $\eta_E = 0.11$.

5   Fig. 6 confirms that, regardless of the particular choice of a single efficiency η, the decrease of precipitation over wetter soils cannot be captured. In contrast, using the two efficiencies η_A and η_E gives a much better match with the simulated value of P_{dry} (see blue line in Fig. 6). Also, by using two efficiencies, the latter become independent of soil moisture. The efficiencies can be alternatively estimated through a fit of Eq. 2 using all the values of A_{dry} and E_{dry} in Tab. 2. In this case we obtain the values $\eta_A = 0.15$ and $\eta_E = 0.10$ which, as expected, do not differ much from the ones computed using the two extreme cases.

10 The fact that one efficiency is not enough to describe the variations of precipitation, in contrast to previous studies, may be linked to the fact that we consider a small domain and a short time scale. The assumption of a well-mixed atmosphere likely holds better on a continental (e.g. Europe) and seasonal scale, as in Schär et al. (1999). Using two efficiencies nevertheless requires data from at least two simulations with different values of advection, evaporation and precipitation.

Initializing the atmosphere with a different sounding will likely lead to different efficiencies. This is illustrated with the `ID_`

15 cases (see Tab. 3), where the idealized sounding of Schlemmer et al. (2012) is used to initialize the atmosphere (see section 2). For a given soil moisture, advection reaches smaller value that in the `DA` case. This is mainly an effect of larger precipitation amounts that fall on the wet patch which in turn prevents an efficient advection of moisture from the wet to the dry patch.

The efficiencies computed for this case range from 47% to 31%, indicating that the atmosphere is more efficient at converting

Case	A_{dry}	E_{dry}	P_{dry}	η
ID_20_100	3.814	0.008	1.789	0.468
ID_30_100	3.861	0.028	1.912	0.492
ID_40_100	3.920	0.143	1.671	0.411
ID_50_100	3.557	0.659	1.740	0.413
ID_60_100	2.631	2.054	1.759	0.376
ID_70_100	0.865	4.080	1.542	0.312
ID_80_100	-0.068	4.884	1.652	0.334
ID_100_100	0.022	4.776	1.662	0.346

Table 3. As in Tab. 2 but for the ID sounding.

advection and evaporation into precipitation than in DA. The higher efficiencies obtained with the ID sounding are due to a combination of different effects. One of those is the different convection triggering. With the ID sounding convection is triggered almost 1 hour before than with the DA sounding (not shown). This allows the atmosphere to fully exploit the instability caused by the morning heating which manifests itself in a stronger enhancement of precipitation at the front, as shown in Fig. 7. This is also corroborated by the fact that CAPE at 15 LST is larger than the one at the initial time over both patches in DA_20_100 whereas it is depleted over the dry patch in the ID_20_100 case (not shown). Moreover, as indicated by Fig. 2, the dew-point depression in the ID sounding is smaller than in the DA sounding throughout most of the atmospheric column. This suggests that, in the ID case, convective updrafts are less affected by the entrainment of environmental dry air. We verify this by computing the average difference in Moist Static Energy (MSE) between updrafts, defined as grid points with vertical velocity greater than 1 m s^{-1} and cloud water content greater than 10^{-4} kg kg^{-1}, and the environment (not shown). Results show that this difference in the ID case is less than 50 % the values observed in the DA case.

Despite the differences, the ID case confirms that advection and evaporation exhibit distinct efficiencies and that precipitation decreases with increased local soil moisture. Here the decrease of precipitation is smaller than the one obtained in the DA_ cases. Although this could be related to a weaker sensitivity of the ID atmospheric state to modifications in the land-surface heterogeneity, we note that the amount of precipitation strongly depends on the collision of the fronts. As shown in Fig. 7 the collision of the fronts in the center of the dry patch has different effects on precipitation depending on the atmospheric state. In the ID_20_100 case strong precipitation events with local maxima of 10 mm h^{-1} are produced in the center of the patch after the fronts' collision and several secondary events develop due to the fronts propagating away from the collision. Instead, in the DA_20_100 case, no strong precipitation event is produced when the fronts collide.

4 Theoretical model

In section 3.2 we showed that precipitation can be expressed as a linear combination of advection and evaporation weighted by different efficiencies which are assumed independent of soil moisture (Eq. 2). Knowing this we can now try to answer
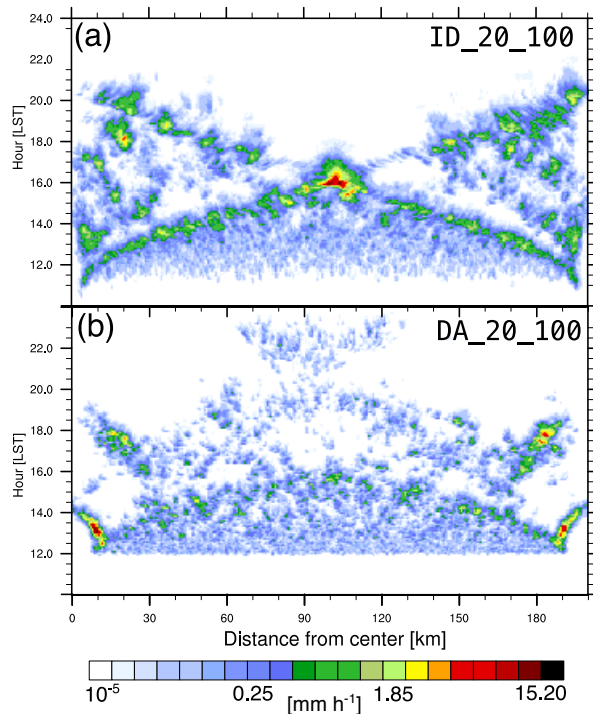
Figure 7. Hovmöller diagram of precipitation rate [mm h^{-1}] in case `ID_20_100` and `DA_20_100`.

one of the first question that was posed in the introduction: What are the minimum parameters that control the variation of precipitation with soil moisture? In order to do so we first have to derive some functional forms of evaporation and advection in terms of soil moisture.

4.1 Surface evaporation

5 The simplest parametrization of evaporation (we will neglect the transpiration part given that our study does include plants) is the so-called *bucket model* introduced by Budyko (1961) and extended by Manabe (1969). Evaporation is defined as a potential term controlled by a limiting factor (also called stress factor). Here we use such a formulation to approximate first the surface latent heat flux LH [mm h^{-1}] at a certain point in space and time as a function of soil moisture ϕ [m^3 m^{-3}]:

$$
\text{LH}(\phi) = \mathcal{A}Q_{\text{net}} \times
\begin{cases}
0 & \text{for } \phi < \phi_{\text{wp}} \\
\frac{\phi - \phi_{\text{wp}}}{\phi_{\text{crit}} - \phi_{\text{wp}}} & \text{for } \phi_{\text{wp}} \leq \phi \leq \phi_{\text{crit}} \\
1 & \text{for } \phi > \phi_{\text{crit}}
\end{cases}
\tag{3}
$$

10 where Q_{net} [mm h^{-1}] is the net incoming radiation at the surface (long-wave+short-wave), ϕ_{wp} [m^3 m^{-3}] the soil moisture at the permanent wilting point and ϕ_{crit} [m^3 m^{-3}] is the critical soil moisture at which evaporation does not increase any more with increasing soil moisture. As explained by Seneviratne et al. (2010) this does not usually correspond to the field capacity.

$\mathcal{A}$ is a proportionality constant which needs to be introduced and specified given that, even in the extreme case of a saturated soil, non-zero sensible heat fluxes and ground heat flux prevent the entire conversion of Q_{net} into LH. The constant $\mathcal{A}$ clearly depends on the particular soil model employed as well as on the different parameters that characterize the soil type considered (e.g. albedo, heat capacity) and partially also on the atmosphere.

5   In order to link Eq. 3 to the accumulated evaporation E_{dry} needed in Eq 2 we average Eq. 3 over the dry patch and integrate it over the accumulation period τ. By doing so we assume a constant value for soil moisture and replace it with the value at the initialization time. Such assumption is motivated by the fact that changes in soil moisture over one diurnal cycle are not expected to be able to significantly feed back on evaporation and precipitation on such a short timescale. The assumption is also well justify as the daily average value of soil moisture remains similar to its initial value (not shown). This gives:

$$E_{\text{dry}}(\phi_{\text{dry}}) = \tau \mathcal{A} \langle Q_{\text{net}} \rangle \times \begin{cases} 0 & \text{for } \phi_{\text{dry}} < \phi_{\text{wp}} \\ \frac{\phi_{\text{dry}} - \phi_{\text{wp}}}{\phi_{\text{crit}} - \phi_{\text{wp}}} & \text{for } \phi_{\text{wp}} \leq \phi_{\text{dry}} \leq \phi_{\text{crit}} \\ 1 & \text{for } \phi_{\text{dry}} > \phi_{\text{crit}} \end{cases} \tag{4}$$

where now E_{dry} does not depend on time nor space. $\langle Q_{\text{net}} \rangle$ denotes the net surface incoming radiation averaged over the dry patch and over the period τ, whereas ϕ_{dry} corresponds to the initial value of soil moisture.

Equation 4 can now be used to fit the values of E_{dry} computed from the simulations (Tab. 2) to obtain an unambiguous value for the parameters $\mathcal{A}$, ϕ_{wp} and ϕ_{crit} (see Fig. 8). These are estimated to be $\mathcal{A} = 0.663$, $\phi_{\text{wp}} = 0.213$ m^{3}m^{-3} and $\phi_{\text{crit}} = 0.350$

15   m^{3}m^{-3}. Note that the latter estimate is not far from the field capacity of this soil type, i.e. 0.340 m^{3}m^{-3}, while the estimated wilting point is almost double the expected one, i.e. 0.110 m^{3}m^{-3}. This is related to the fact that the employed bare soil evaporation scheme tends to shut down evaporation too early as noted by Schulz et al. (2016) and Cioni and Hohenegger (2017). Thus, both $\phi_{\text{wp,crit}}$ depend not only on the employed soil type but also on the soil model.

Figure 8 shows the fit of Eq. 4, together with the values obtained in the simulations. It reveals an excellent agreement between

20   theory and simulations. The small discrepancies mainly come from the fact that we assume a constant value of $\langle Q_{\text{net}} \rangle = 300$ W m$^{-2} = 0.43$ mm h^{-1} across the simulations, although the simulated value depends on soil moisture and varies by about 7%. This is due to different cloud regimes which alter the surface radiation balance (Cioni and Hohenegger, 2017, Sec. 4b).

We note that our formulation of evaporation differs from the one used in the model of Lintner et al. (2013) where potential evaporation was used in place of Q_{net}, which is the main difference between the original framework of Budyko (1961) and the

25   one of Manabe (1969).

4.2   Advection

Our goal is to find a formulation of A_{dry} as a function of soil moisture. This can be achieved starting from the definition of Eq. A2 and assuming that the advection of every tracer is mainly due to the propagation of the front associated with the meso-scale
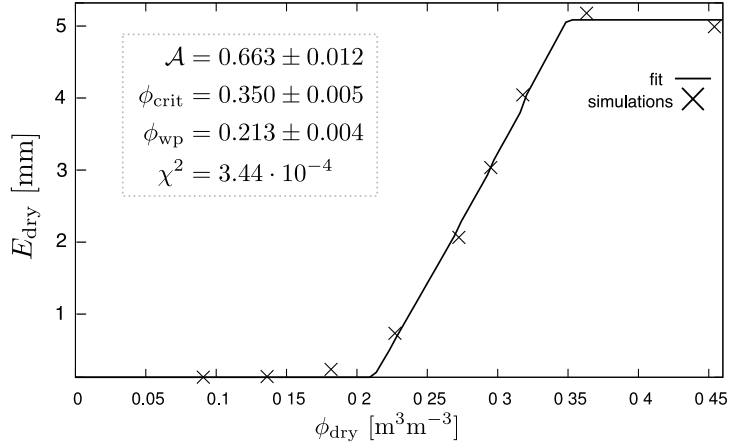
Figure 8. Fit of E_{dry} with values obtained from the simulations of the default configuration (`DA_20_100` to `DA_100_100`). Crosses indicate values obtained from simulations while line indicates the fit performed using Eq. 4. Upper left inset shows the values obtained by the fit together with absolute errors and the residual sum of squares χ^2, i.e. the sum of the squared difference between the values predicted by the fit and the ones obtained in the simulations.

circulation, hence $H = H_{\text{front}}$. In this case

$$A_{\text{dry}} = -\frac{1}{\rho_w} \int\limits_0^\tau \int\limits_0^{H_{\text{front}}} \mathbf{v}_{\text{front}} \cdot \nabla q_{\text{tot}} \Big|_{\text{dry}} \rho_a \, \mathrm{d}z \, \mathrm{d}t \simeq -\frac{1}{\rho_w} \int\limits_0^\tau \int\limits_0^{H_{\text{front}}} u_{\text{front}} \frac{\partial q_{\text{tot}}}{\partial x} \Big|_{\text{dry}} \rho_a \, \mathrm{d}z \, \mathrm{d}t \tag{5}$$

where H_{front} is the height of the front associated with the meso-scale circulation or, equally, the Planetary Boundary Layer (PBL) height, $\mathbf{v}_{\text{front}}$ its speed, ρ_a is the air density and ρ_w the water density. Eq. 5 has been already approximated given that

5 the front propagates mainly in the x direction (see Sec. 3.1), so that there is no y component of ∇q_{tot}.

The propagation speed of the front u_{front} and ρ_a can be seen as constants in the vertical within the height H_{front}, while q_{tot} remains a function of x, z and time t. The time integration can be replaced by considering the average over time multiplied by the time scale τ to obtain

$$A_{\text{dry}} = -\tau \frac{\rho_a}{\rho_w} \langle u_{\text{front}} \rangle_{\text{dry}} \langle \int\limits_0^{H_{\text{front}}} \frac{\partial q_{\text{tot}}}{\partial x} \Big|_{\text{dry}} \mathrm{d}z \rangle = -\tau \frac{\rho_a}{\rho_w} \langle u_{\text{front}} \rangle_{\text{dry}} \langle \int\limits_0^{H_{\text{front}}} \frac{\Delta q_{\text{tot}}}{L_{\text{front}}} \mathrm{d}z \rangle = -\tau \frac{\rho_a}{\rho_w} \langle u_{\text{front}} \rangle_{\text{dry}} \frac{H_{\text{front}}}{L_{\text{front}}} \langle \Delta q_{\text{tot}} \rangle \tag{6}$$

10 In Eq. 6 we approximated the derivative of q_{tot} as the difference between the two patches Δq_{tot} divided by the penetration length of the front, L_{front} (Crosman and Horel, 2010).

To simplify the problem we assume $\Delta q_{\text{tot}} \simeq \Delta q_v$, which is viewed as the difference in specific humidity ahead of the front and behind it. As in studies which have viewed sea breezes as gravity current (Robinson et al., 2013), we assume that this difference is not directly affected by the circulation, which gives an upper bound estimate. The changes in q_v due to surface evaporation

accumulated up to a certain time τ can then be written as

$$q_v(\tau) = q_v(0) + \frac{\rho_w E}{\rho_a H_{\text{moist}}} \Rightarrow \Delta q_v = -\frac{\rho_w}{\rho_a H_{\text{moist}}} \underbrace{(E_{\text{wet}} - E_{\text{dry}})}_{\Delta E} \tag{7}$$

where H_{moist} is the vertical extent of the moistening process due to the accumulated surface evaporation E and $q_v(0)$ is the specific humidity at the initial time. By assuming that the moistening is confined to the PBL, so that $H_{\text{moist}} = H_{\text{front}}$ we can substitute Eq. 7 into Eq. 6 to obtain

$$A_{\text{dry}} = \frac{\tau \langle u_{\text{front}} \rangle}{L_{\text{front}}} \Delta E \tag{8}$$

Our analysis thus indicates that the advection only depends on four terms: τ, which is a constant, the difference in E between the two patches, which can be estimated from Eq. 4 and which depends on the soil moisture, as well as L_{front} and u_{front}. In all simulations the front has a constant inland propagation of $L_{\text{front}} \simeq 100$ km, which corresponds to half of the patch size. More importantly, the front speed does not vary much with different surface heterogeneity gradients, against our initial expectations that motivated this study (see Introduction). For example, between the DA_20_100 and the DA_60_100 cases only a 3% relative decrease in the front speed is observed (not shown).

This counter intuitive behaviour is related to the fact that cold pools lead to a noticeable acceleration of the front, as seen in section 3.1. Although the front is initially triggered by the surface heterogeneity, and different surface heterogeneities may lead to different initial propagation velocities, the much faster cold pools end up determining the front velocity, thus masking the effect of the surface heterogeneity. This stands in agreement with what found by Rieck et al. (2015), and in particular with the thermodynamic contribution of cold pools to the propagation speed of the front (their Eq. 1). Moreover, cold pools are distributed along the front and continuously fed by precipitation events, similarly to what happens in squall-lines. Given this spatial organization, their strength and propagation do not depend on the surface state, as in the case for isolated convection (Gentine et al., 2016). Instead they solely depend on the state of the mid- to upper-troposphere (Peters and Hohenegger, 2017) which is also not significantly modified by surface fluxes over the course of one diurnal cycle.

We can thus finally express advection simply as

$$A_{\text{dry}}(\phi_{\text{dry}}) = \mathcal{B} \Delta E(\phi_{\text{dry}}) \tag{9}$$

where $\mathcal{B} = \tau \langle u_{\text{front}} \rangle / L_{\text{front}}$ is a proportionality constant that does not depend on soil moisture. Using the parameters $\mathcal{A}, \phi_{\text{wp}}, \phi_{\text{crit}}$ obtained from the fit of Eq. 4 (see Fig. 8) we can compute the difference $\Delta E(\phi_{\text{dry}})$. Together with the values of A_{dry} obtained in the simulations the values of $\Delta E(\phi_{\text{dry}})$ can be used to fit Eq. 9 and compute a value for the parameter $\mathcal{B}$: in the DA cases $\mathcal{B} = 1.47$. This is smaller than the value that would be obtained by estimating instead $\langle u_{\text{front}} \rangle$ and L_{front} directly, as this latter approximation does not take into account moisture losses due to advection.

Figure 9 shows the values of A_{dry} and the fit performed using Eq. 9 for the basic set of experiments and for further cases, the latter used to test the finding that $\mathcal{B}$ does not depend on ϕ but solely on the atmospheric state. Overall the fit matches the variation of A_{dry} with ϕ_{dry} remarkably well given the various assumptions. Both the simulated decrease of A_{dry} with higher
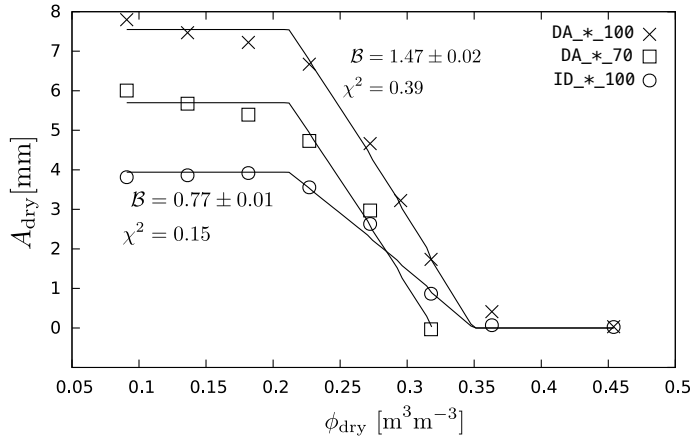
Figure 9. Fit of the advection in cases `DA_*_100`, `DA_*_70` and `ID_*_100`. Symbols indicate the values obtained from the simulations while lines represent the fit performed using Eq. 9. The obtained values of $\mathcal{B}$ are reported in the insets, together with the absolute error and the χ^2 value (see Fig. 8 for the definition). Note that for the `DA_*_100` and `DA_*_70` cases the fits yielded similar results: for this reason the obtained value for $\mathcal{B}$ is reported only once.

values of soil moisture and the flattening of advection by soil moisture lower than the wilting point are reproduced, although both effects seem to be overestimated by Eq. 9.

In the simulations where the initial value of ϕ_{wet} is reduced to just 70% of saturation the estimated value of $\mathcal{B}$ is almost the same as the one of the default configuration, confirming that $\mathcal{B}$ does not depend on soil moisture. Instead, in the `ID_` cases

5 (Tab. 3), which use a different atmospheric profile and hence support distinct cold pool strength, the value of $\mathcal{B}$ is reduced by about half.

4.3 Computing the derivative of precipitation

Equations 2, 4 and 9 can be combined in order to compute P_{dry}. We are, however, interested in its variation with soil moisture, $\frac{\partial P_{\mathrm{dry}}}{\partial \phi_{\mathrm{dry}}}$, which can be computed as:

$$
\begin{aligned}
\frac{\partial P_{\mathrm{dry}}}{\partial \phi_{\mathrm{dry}}} &= \eta_A \frac{\partial A_{\mathrm{dry}}}{\partial \phi_{\mathrm{dry}}} + \eta_E \frac{\partial E_{\mathrm{dry}}}{\partial \phi_{\mathrm{dry}}} \\
&= \eta_A \frac{\partial}{\partial \phi_{\mathrm{dry}}} \left(\mathcal{B} \left(E_{\mathrm{wet}} - E_{\mathrm{dry}} \right) \right) + \eta_E \frac{\partial E_{\mathrm{dry}}}{\partial \phi_{\mathrm{dry}}} \\
&= -\eta_A \mathcal{B} \frac{\partial E_{\mathrm{dry}}}{\partial \phi_{\mathrm{dry}}} + \eta_E \frac{\partial E_{\mathrm{dry}}}{\partial \phi_{\mathrm{dry}}}
\end{aligned}
\tag{10}
$$

Note that the derivation of Eq. 10 retains only one term of the difference given that E_{wet} does not depend on ϕ_{dry}. Using Eq. 4 it is straightforward to compute the derivative of E_{dry} as

$$\frac{\partial E_{\text{dry}}}{\partial \phi_{\text{dry}}} = \tau \mathcal{A} \langle Q_{\text{net}} \rangle \times \begin{cases} 0 & \text{for } \phi_{\text{dry}} < \phi_{\text{wp}} \\ (\phi_{\text{crit}} - \phi_{\text{wp}})^{-1} & \text{for } \phi_{\text{wp}} \leq \phi_{\text{dry}} \leq \phi_{\text{crit}} \\ 0 & \text{for } \phi_{\text{dry}} > \phi_{\text{crit}} \end{cases} \tag{11}$$

which is a step-wise function constituted by constant values.

5   Equations 10 and 11 indicate that for $\phi_{\text{dry}} < \phi_{\text{wp}}$ and $\phi_{\text{dry}} > \phi_{\text{crit}}$ there is no change in precipitation with soil moisture independently of the value of the efficiencies. In contrast for $\phi_{\text{wp}} \leq \phi_{\text{dry}} \leq \phi_{\text{crit}}$ then $\frac{\partial E_{\text{dry}}}{\partial \phi_{\text{dry}}} \neq 0$ but still the derivative of precipitation with respect to soil moisture does not depend upon the soil moisture content itself. These findings contrast with the ones of Lintner et al. (2013), who found a minimum of the derivative for intermediate values of soil moisture. This is a consequence of the formulation of E_{dry} as a linear function of ϕ_{dry} and the fact that A_{dry} also turned out to be a linear function of ϕ_{dry} as u_{front}

10   is constant. This remains true as long as the convection is strongly organized by the front associated with the meso-scale circulation and produces strong cold pools that end up determining the propagation velocity. It should be noted that, although the derivative $\frac{\partial P_{\text{dry}}}{\partial \phi_{\text{dry}}}$ does not depend on soil moisture, the absolute value of precipitation P_{dry} does indeed depend on soil moisture, as we will shown later.

Coming back to Eqs. 10 and 11, we can now determine under which conditions P_{dry} will increase or decrease.

15    $$\frac{\partial P_{\text{dry}}}{\partial \phi_{\text{dry}}} \lessgtr 0 \Leftrightarrow -\eta_A \mathcal{B} + \eta_E \lessgtr 0 \Leftrightarrow \eta_E \lessgtr \eta_A \mathcal{B} \tag{12}$$

The atmospheric conditions, through the terms η_A, η_E and $\mathcal{B}$, determine whether increasing or decreasing the soil moisture of the dry patch is needed to increase the precipitation amount. Inserting the values of the efficiencies and of $\mathcal{B}$ obtained from the `DA_` simulations in Eq. 12 confirms that $\frac{\partial P_{\text{dry}}}{\partial \phi_{\text{dry}}} < 0$, which agrees with the simulated increase of precipitation with decreasing values of soil moisture. These results are generalized with the help of Fig. 10 for three different values of $\mathcal{B}$.

20   In Fig. 10 positive values indicate an increase of precipitation over the dry patch with soil moisture, and vice-versa. Not surprisingly (see Eq. 12) using a value of $\mathcal{B} = 1$ gives a symmetric picture where an increase of precipitation with soil moisture is obtained for those cases when $\eta_E > \eta_A$. This relationship is modified by the value of $\mathcal{B}$.

Figure 10 overall shows that, as long as $\eta_A > \eta_E$ it is very unlikely to get a positive derivative. Only with values of $\mathcal{B}$ small enough, which would mean weaker and slower cold pools, the derivative may change sign even with $\eta_A > \eta_E$. This situation

25   almost happens in the `ID` simulation, where the theory predicts a derivative close to zero. This agrees with the weaker sensitivity of precipitation to soil moisture observed in that case. Alternatively, to get a positive derivative, evaporation should become much more efficient than advection, i.e. $\eta_E \gg \eta_A$. This, however, did not happen in the performed simulations.

These findings already answer the main question posed in the introduction and can be further generalized to the case when both ϕ_{wet} and ϕ_{dry} are changed at the same time. This allows one to investigate the dependency of precipitation on the soil

30   moisture values of the two patches when the η_A, η_E and $\mathcal{B}$ parameters are fixed. First of all, $\frac{\partial P_{\text{dry}}}{\partial \phi_{\text{wet}}}$ can be computed with the
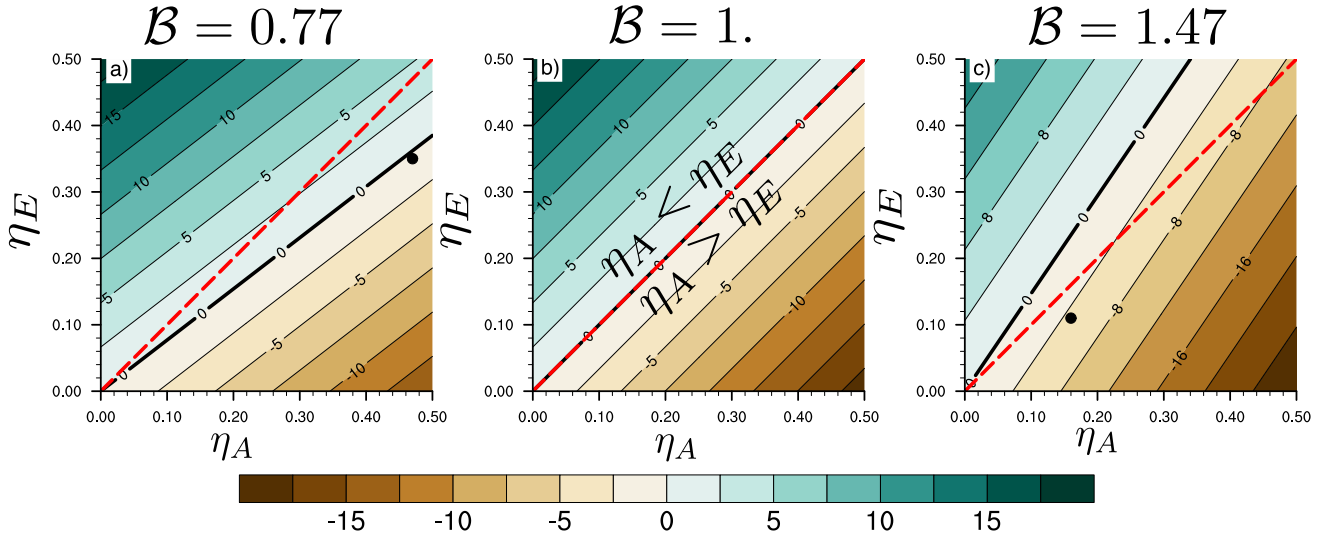
Figure 10. Contour plot of $\frac{\partial P_\text{dry}}{\partial \phi_\text{dry}}$ [mm m^3 m^{-3}] as a function of η_A, η_E for different values of the parameter $\mathcal{B}$. The black points in (a) and (c) are placed using the efficiencies obtained in the `ID_` and `DA_` cases, respectively. The dashed red line distinguishes the areas where $\eta_A > \eta_E$ and vice versa. Note the symmetric color scale and the thicker zero contour line.

same method as before:

$$\frac{\partial P_\text{dry}}{\partial \phi_\text{wet}} = \eta_A \mathcal{B} \frac{\partial E_\text{wet}}{\partial \phi_\text{wet}} \tag{13}$$

given that the evaporation over the dry patch does not depend on the soil moisture of the wet patch. Second, the two derivatives $\frac{\partial P_\text{dry}}{\partial \phi_\text{wet}}, \frac{\partial P_\text{dry}}{\partial \phi_\text{dry}}$ can be combined to obtain the total precipitation change on the dry patch.

$$\begin{aligned}
\Delta P_\text{dry} &= \frac{\partial P_\text{dry}}{\partial \phi_\text{dry}} \Delta \phi_\text{dry} + \frac{\partial P_\text{dry}}{\partial \phi_\text{wet}} \Delta \phi_\text{wet} \\
&= (\eta_E - \eta_A \mathcal{B}) \frac{\partial E_\text{dry}}{\partial \phi_\text{dry}} \Delta \phi_\text{dry} + \eta_A \mathcal{B} \frac{\partial E_\text{wet}}{\partial \phi_\text{wet}} \Delta \phi_\text{wet}
\end{aligned} \tag{14}$$

Assuming that the soil type of both patches is the same, only the case $\phi_\text{wp} < \phi_\text{dry,wet} < \phi_\text{crit}$ is of interest. The other cases either revert to the previously discussed case (Eq. 12) or reduce to the trivial solution where only $\Delta \phi_\text{wet}$ is affecting ΔP_dry. For $\phi_\text{wp} < \phi_\text{dry,wet} < \phi_\text{crit}$ we obtain $\frac{\partial E_\text{dry}}{\partial \phi_\text{dry}} = \frac{\partial E_\text{wet}}{\partial \phi_\text{wet}}$. Thus, changes in precipitation in our idealized model can be formulated as

$$\Delta P_\text{dry} = \tau \frac{\mathcal{A} \langle Q_\text{net} \rangle}{\phi_\text{crit} - \phi_\text{wp}} \left((\eta_E - \eta_A \mathcal{B}) \Delta \phi_\text{dry} + \eta_A \mathcal{B} \Delta \phi_\text{wet} \right) \tag{15}$$

10   The behaviour of Eq. 15 as function of $\Delta \phi_\text{dry}, \Delta \phi_\text{wet}$ and $\mathcal{B}$ is investigated with the help of Fig. 11. In the default configuration described in section 3.1 the soil moisture of the wet patch was kept constant, i.e. $\Delta \phi_\text{wet} = 0$, while the soil moisture of the dry patch was increased, i.e. $\Delta \phi_\text{dry} > 0$. Figure 11 (a) shows that, in the aforementioned case, ΔP_dry is negative, as in our simulations. In this case decreasing ϕ_dry and increasing ϕ_wet is the most efficient way to increase precipitation.
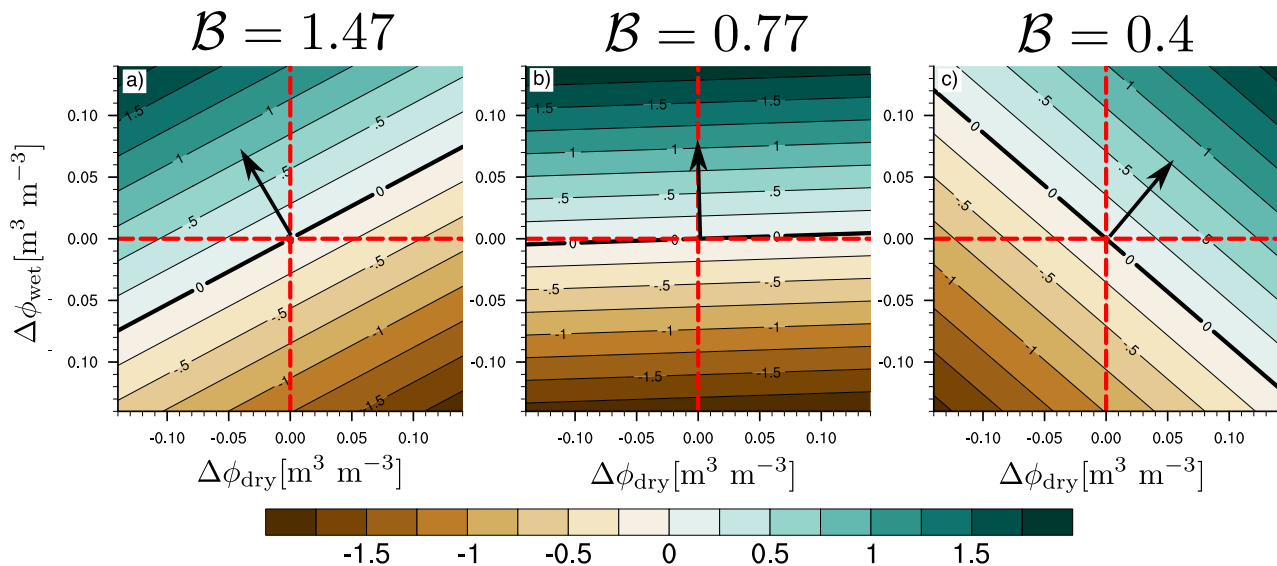
Figure 11. ΔP_{dry} as function of $\Delta\phi_{\text{dry}}$ and $\Delta\phi_{\text{wet}}$ for different values of the parameter $\mathcal{B}$. The x and y axes represent the variation of ϕ_{dry} and ϕ_{wet}, respectively. Note that the maximum variation is $\phi_{\text{crit}} - \phi_{\text{wp}}$, as ΔP_{dry} is computed for the regime $\phi_{\text{wp}} < \phi_{\text{dry,wet}} < \phi_{\text{crit}}$. The red dashed lines indicate no variation of the soil moisture of either one of the patches. The efficiencies are set to $(\eta_A, \eta_E) = (0.16, 0.11)$ in (a) and to $(\eta_A, \eta_E) = (0.47, 0.35)$ in (b) and (c) to match the simulation results. The black arrow indicates the direction of maximum growth, i.e. when an increase of precipitation is expected.

Figure 11 (b) presents the case characteristic of the simulations performed with the `ID` sounding. The flattening of the contour lines shows that there is little sensitivity on ϕ_{dry}, as previously discussed. Mainly increasing ϕ_{wet} would allow precipitation to increase. In the extreme case where $\mathcal{B}$ is further reduced (Fig. 11 c) the picture partly reverses. Both soil moisture of the wet and of the dry patch should be increased to sustain an increase of precipitation, as evaporation becomes now relevant and advection has a negligible contribution.

Figure 11 thus indicates that, in any case, the soil moisture of the wet patch should be increased to get more precipitation on the dry patch. The response to changes in soil moisture of the dry patch is more subtle, and the combination of the two responses can lead to positive or negative coupling depending on the atmosphere state. This may explain why in reality both signs of the coupling are observed with different atmospheric states.

5 Conclusions

Motivated by the ambiguous relationship between soil moisture, soil moisture heterogeneity and precipitation we designed idealized simulations of a convective diurnal cycle that make use of a coupled configuration of an atmospheric Large Eddy Simulation (LES) model and a land-surface model. The heterogeneity in the land surface was prescribed by dividing the do-

main into two patches with different initial values of soil moisture. Inspired by the results of the simulations, we specifically wanted to derive a simple conceptual model that retains the minimum parameters that control precipitation over a spatially drier patch. Moreover, we wanted to use this model to understand which is the most efficient way to increase precipitation by acting on soil moisture given the opposite control of soil moisture on advection and evaporation.

5 Since the main potential sources contributing to precipitation are constituted by remote moisture advection by the meso-scale circulation triggered by the soil moisture heterogeneity and local evaporation, we first aim at disentangling the effects of these two on precipitation. Results from the simulations show, as expected, that the moisture advection over the dry patch decreases with increasing local soil moisture, while evaporation increases. The interplay between these two effects produces a decrease of precipitation with increasing values of local soil moisture for the considered case.

10 More importantly the simulation results indicated that such a decrease can only be correctly reproduced by assuming that advection and evaporation processes contribute differently to precipitation. Hence we model precipitation as the sum of advection and evaporation each weighted by its own efficiency (see Eq. 2). By using two efficiencies they become independent of soil moisture and only dependent on the initial atmospheric state.

As a second step we conceptualize the variations of evaporation and advection with soil moisture. Evaporation can be approxi-

15 mated using the *bucket* model owing to Budyko (1961) (see Eq. 3). The advection is estimated as the product of the breeze front velocity and the gradient in near-surface specific humidity (see Eq. 5). A priori we would have expected a squared dependency of advection on soil moisture since both the velocity of the front and the gradient in specific humidity should be related to soil moisture. However, it turns out that the velocity of the front is independent of soil moisture as the development of convection at the breeze front and the generation of strong cold pools lead to a strong acceleration of the front that fully masks the effect

20 of the initial surface heterogeneity.

Putting all the results together indicates that the derivative of precipitation with respect to the soil moisture of the dry patch does not depend on the actual soil moisture value. This is due to the fact that the functional forms of advection and evaporation ends up to be linear functions in soil moisture. The idealized model is valid as long as the evaporation keeps its linearity as function of soil moisture and the propagation speed of the front does not depend on the surface heterogeneity gradient, meaning

25 strong enough cold pools.

The parameters that control the variations of precipitation with local soil moisture are the aforementioned efficiencies and a scale parameter that defines the magnitude of the advection. All these parameters depend solely on the atmospheric state. According to the values of these parameters, as estimated from the simulations, the most efficient way to increase precipitation over the dry patch is to decrease the soil moisture of the dry patch. Thus, one can say that, in order to have more precipitation

30 over spatially drier areas, more precipitation should first fall on spatially wetter ones. In other words, the most efficient way to obtain more precipitation over dry areas is to let them dry out for a long time so that a stronger gradient can build up and thus produce more explosive convective events due to a stronger meso-scale circulation.

However, if either the efficiency of evaporation becomes much larger than the one of advection or the scale parameter that defines the importance of advection decreases under a certain threshold then the response of precipitation can be reversed.

35 Although we did not find any evidence of this behaviour for the two atmospheric profiles tested in this work it would be inter-

esting as a next step to derive the three parameters predicted by the conceptual model from more realistic simulations to infer the frequency of occurrence of the various precipitation regimes.

Appendix A: Computation of the advection as residual term

The advection of every tracer is computed directly from the moisture balance equation as a residual. We use the following formulation, which applies for a certain point (x, y) over a 2-dimensional domain:

$$\frac{1}{\rho_w} \int_0^\tau \int_0^H \frac{\mathrm{D}q_{\mathrm{tot}}}{\mathrm{D}t} \rho_a \, \mathrm{d}z \, \mathrm{d}t = \frac{1}{\rho_w} \int_0^\tau \int_0^H \left[\frac{\partial q_{\mathrm{tot}}}{\partial t} + \mathbf{v} \cdot \nabla q_{\mathrm{tot}} \right] \rho_a \, \mathrm{d}z \, \mathrm{d}t = E - P \tag{A1}$$

where D indicates the total derivative, P [m] is the accumulated precipitation, E [m] the accumulated evaporation, q_{tot} [kg kg^{-1}] represents the sum of all tracers (water vapour q_v, clouds q_c, rain q_r, snow q_s, ice q_i, graupel q_g and hail q_h) mixing ratios, ρ_w [kg m^{-3}] the density of water, ρ_a [kg m^{-3}] the air density and $\mathbf{v}$ the velocity of air as a vector. H indicates the top of the simulation domain and τ the lenght of the accumulation period (18 hours in our experiments). The total derivative can be divided into its advective term:

$$A \equiv -\frac{1}{\rho_w} \int_0^\tau \int_0^H \mathbf{v} \cdot \nabla q_{\mathrm{tot}} \rho_a \, \mathrm{d}z \, \mathrm{d}t \tag{A2}$$

and the local derivative:

$$\frac{1}{\rho_w} \int_0^\tau \int_0^H \frac{\partial q_{\mathrm{tot}}}{\partial t} \rho_a \, \mathrm{d}z \, \mathrm{d}t = A + E - P \tag{A3}$$

In both equations A2 and A3 the variables A, E, P are solely functions of (x, y) whereas q_{tot} depends also on time t and on the vertical coordinate z. We can eliminate the dependency on (x, y) by applying an average operator over a certain area, indicated with the subscript $_{\mathrm{area}}$:

$$\frac{1}{\rho_w} \int_0^\tau \int_0^H \frac{\partial q_{\mathrm{tot}}}{\partial t} \bigg|_{\mathrm{area}} \rho_a \, \mathrm{d}z \, \mathrm{d}t = A_{\mathrm{area}} + E_{\mathrm{area}} - P_{\mathrm{area}} \tag{A4}$$

In the main text we use as area either the full domain, denoted with the suffix $_{\mathrm{dom}}$, or the dry patch only, denoted by the suffix $_{\mathrm{dry}}$. By indicating the weighted vertical integral of q_{tot} as $\overline{q}_{\mathrm{tot}} \equiv \int_0^H q_{\mathrm{tot}} \rho_a \, \mathrm{d}z$ we can further simplify the previous equation to:

$$\frac{1}{\rho_w} \int_0^\tau \frac{\partial \overline{q}_{\mathrm{tot}}}{\partial t} \bigg|_{\mathrm{area}} \mathrm{d}t = A_{\mathrm{area}} + E_{\mathrm{area}} - P_{\mathrm{area}} \tag{A5}$$

Although other studies only considered the advection of water vapour, i.e. of $\overline{q}_v$, in order to close the balance it is necessary to consider all species. In fact, although $\overline{q}_i, \overline{q}_g, \overline{q}_h, \overline{q}_s$ are order of magnitudes smaller than $\overline{q}_v, \overline{q}_c, \overline{q}_r$, their variations over time are not, so that neglecting these terms in Eq. A5 would lead to an unbalance.

From the 5-min simulation output we use Eq. A5 and estimate the advection as the residual $R_{\mathrm{area}} = \frac{1}{\rho_w} \int_0^\tau \frac{\partial \overline{q}_{\mathrm{tot}}}{\partial t}\Big|_{\mathrm{area}} \mathrm{d}t + P_{\mathrm{area}} - E_{\mathrm{area}} \equiv A_{\mathrm{area}}$. We verify that, when averaged over the entire domain, $R_{\mathrm{dom}} = 0$.

Competing interests. The authors declare that they have no competing interests.

Acknowledgements. This research was supported by the Hans-Ertel-Zentrum for Weather Research (HErZ), a collaborative project involving universities across Germany, the Deutscher Wetterdienst (DWD) and funded by the Federal Ministry of Transport and Digital Infrastructure (BMVI). The simulations were performed using the facilities of the Deutsches Klimarechenzentrum (DKRZ) and in particular the new supercomputer *Mistral*. Primary data and scripts used in the analysis are archived by the Max Planck Institute for Meteorology and can be obtained by contacting publications@mpimet.mpg.de.

References

Avissar, R. and Liu, Y.: Three-dimensional numerical study of shallow convective clouds and precipitation induced by land surface forcing, Journal of Geophysical Research: Atmospheres, 101, 7499–7518, 1996.

Budyko, M.: Climate and Life, Academic Press, New York, 1974.

Budyko, M. I.: The heat balance of the earth's surface, Soviet Geography, 2, 3–13, 1961.

Chen, F. and Avissar, R.: Impact of land-surface moisture variability on local shallow convective cumulus and precipitation in large-scale models, Journal of Applied Meteorology, 33, 1382–1401, 1994.

Cioni, G. and Hohenegger, C.: Effect of soil moisture on diurnal convection and precipitation in Large-Eddy Simulations, Journal of Hydrometeorology, 2017.

Crosman, E. T. and Horel, J. D.: Sea and lake breezes: a review of numerical studies, Boundary-layer meteorology, 137, 1–29, 2010.

Doms, G., Forstner, J., Heise, E., Herzog, H.-J., Mironov, D., Raschendorfer, M., Reinhardt, T., Ritter, B., Schrodin, R., Schulz, J.-P., and Vogel, G.: A Description of the Nonhydrostatic Regional COSMO Model. Part II: Physical Parametrization, Consortium for Small-Scale Modeling, 2011.

Findell, K. L. and Eltahir, E. A.: Atmospheric controls on soil moisture-boundary layer interactions. Part I: Framework development, Journal of Hydrometeorology, 4, 552–569, 2003.

Froidevaux, P., Schlemmer, L., Schmidli, J., Langhans, W., and Schär, C.: Influence of the background wind on the local soil moisture–precipitation feedback, Journal of the Atmospheric Sciences, 71, 782–799, 2014.

Gentine, P., Garelli, A., Park, S.-B., Nie, J., Torri, G., and Kuang, Z.: Role of surface heat fluxes underneath cold pools, Geophysical research letters, 43, 874–883, 2016.

Guillod, B. P., Orlowsky, B., Miralles, D. G., Teuling, A. J., and Seneviratne, S. I.: Reconciling spatial and temporal soil moisture effects on afternoon rainfall, Nature communications, 6, 2015.

Koster, R. D., Dirmeyer, P. A., Guo, Z., Bonan, G., Chan, E., Cox, P., Gordon, C., Kanae, S., Kowalczyk, E., Lawrence, D., et al.: Regions of strong coupling between soil moisture and precipitation, Science, 305, 1138–1140, 2004.

Lintner, B. R., Gentine, P., Findell, K. L., D'Andrea, F., Sobel, A. H., and Salvucci, G. D.: An idealized prototype for large-scale land–atmosphere coupling, Journal of Climate, 26, 2379–2389, 2013.

Lynn, B. H., Tao, W.-K., and Wetzel, P. J.: A study of landscape-generated deep moist convection, Monthly weather review, 126, 928–942, 1998.

Manabe, S.: Climate and the ocean circulation 1: i. The atmospheric circulation and the hydrology of the earth's surface, Monthly Weather Review, 97, 739–774, 1969.

Neelin, J. D. and Zeng, N.: A quasi-equilibrium tropical circulation model—Formulation, Journal of the atmospheric sciences, 57, 1741–1766, 2000.

Peters, K. and Hohenegger, C.: On the Dependence of Squall-Line Characteristics on Surface Conditions, Journal of the Atmospheric Sciences, 74, 2211–2228, 2017.

Rieck, M., Hohenegger, C., and Gentine, P.: The effect of moist convection on thermally induced mesoscale circulations, Quarterly Journal of the Royal Meteorological Society, 141, 2418–2428, 2015.

Robinson, F., Patterson, M. D., and Sherwood, S.: A numerical modeling study of the propagation of idealized sea-breeze density currents, Journal of the Atmospheric Sciences, 70, 653–668, 2013.

Robinson, F. J., Sherwood, S., and Li, Y.: Resonant response of deep convection to surface hot spots, Journal of the Atmospheric Sciences, 65, 276–286, 2008.

Schär, C., Lüthi, D., Beyerle, U., and Heise, E.: The soil-precipitation feedback: A process study with a regional climate model, Journal of Climate, 12, 722–741, 1999.

5 Schlemmer, L., Hohenegger, C., Schmidli, J., and Schär, C.: Diurnal equilibrium convection and land surface-atmosphere interactions in an idealized cloud-resolving model, Quarterly Journal of the Royal Meteorological Society, 138, 1526–1539, 2012.

Schulz, J.-P., Vogel, G., Becker, C., Kothe, S., Rummel, U., and Ahrens, B.: Evaluation of the ground heat flux simulated by a multi-layer land surface scheme using high-quality observations at grass land and bare soil, Meteorologische Zeitschrift, pp. –, https://doi.org/10.1127/metz/2016/0537, http://dx.doi.org/10.1127/metz/2016/0537, 2016.

10 Segal, M. and Arritt, R.: Nonclassical mesoscale circulations caused by surface sensible heat-flux gradients, Bulletin of the American Meteorological Society, 73, 1593–1604, 1992.

Seneviratne, S. I., Corti, T., Davin, E. L., Hirschi, M., Jaeger, E. B., Lehner, I., Orlowsky, B., and Teuling, A. J.: Investigating soil moisture–climate interactions in a changing climate: A review, Earth-Science Reviews, 99, 125–161, 2010.

Taylor, C. M., de Jeu, R. A., Guichard, F., Harris, P. P., and Dorigo, W. A.: Afternoon rain more likely over drier soils, Nature, 489, 423–426, 15 2012.

Tuttle, S. and Salvucci, G.: Confounding factors in determining causal soil moisture-precipitation feedback, Water Resources Research, 2017.

Wei, J., Su, H., and Yang, Z.-L.: Impact of moisture flux convergence and soil moisture on precipitation: a case study for the southern United States with implications for the globe, Climate dynamics, 46, 467, 2016.

20 Yan, H. and Anthes, R. A.: The effect of variations in surface moisture on mesoscale circulation, Monthly Weather Review, 116, 192–208, 1988.

Zängl, G., Reinert, D., Rípodas, P., and Baldauf, M.: The ICON (ICOsahedral Non-hydrostatic) modelling framework of DWD and MPI-M: Description of the non-hydrostatic dynamical core, Quarterly Journal of the Royal Meteorological Society, 141, 563–579, 2015.